Beamforming method for extracting the broadband noise sources of counter-rotating open rotors

Kristóf Tokaji,[1] Bálint Soós,[2] Csaba Horváth[3]

Budapest University of Technology and Economics

Budapest, H-1111, Hungary

Counter-Rotating Open Rotors (CROR) are known to have advantageous propulsive efficiency properties, but at the same time many noise emission issues related to this technology still need to be investigated. The noise they generate consists of tonal and broadband components, of which the tonal components often appear in narrow frequency bands with large amplitudes. During beamforming investigations this often makes sorting them out from among other noise sources in the same frequency bin rather straight forward. On the other hand, the broadband noise sources can be characterized as having small amplitudes, and in general they are not the dominant noise sources in many frequency bins, but overall a significant noise component that needs to be investigated. The literature has provided a single microphone signal pre-processing method for removing the tonal components and hence isolating the broadband noise of a CROR, the signal of which has been shown to be appropriate for the investigation of broadband spectra. In this article, this pre-processing method is further developed into a beamforming method which can be used in order to localize the broadband noise sources of CROR. The resulting beamforming maps have been compared to the results of earlier broadband noise CROR studies, showing the

---

[1] PhD student, Department of Fluid Mechanics, Faculty of Mechanical Engineering, Budapest University of Technology and Economics, 1111 Budapest, Bertalan Lajos utca 4-6, Hungary, tokaji@ara.bme.hu.

[2] Student, Department of Fluid Mechanics, Faculty of Mechanical Engineering, Budapest University of Technology and Economics, 1111 Budapest, Bertalan Lajos utca 4-6, Hungary, soosba94@gmail.com.

[3] Assistant professor, Department of Fluid Mechanics, Faculty of Mechanical Engineering, Budapest University of Technology and Economics, 1111 Budapest, Bertalan Lajos utca 4-6, Hungary, horvath@ara.bme.hu, AIAA member.

validity of the new method and the advantages of using it as compared to methods used in other investigations.

I. Nomenclature

A. Latin letters

A = *Blade passing frequency of the aft rotor (Hz)*

D = *Number of periods defined by the frequency of the non-rotational noise source*

F = *Rotational frequency*

f = *Frequency of the non-rotational noise source*

f_s = *Sampling frequency*

M_x = *Mach number in the wind tunnel*

n = *Number of segments of the non-rotational noise source filtering*

S = *Number of data points in a segment*

X = *The first segment of the rotational noise source filtering*

x = *The first segment of the non-rotational noise source filtering*

Y = *The second segment of the rotational noise source filtering*

y = *The second segment of the non-rotational noise source filtering*

Z = *A segment of the Single filtered signal*

z = *A segment of the Double filtered signal*

B. Subscripts, superscripts and others

1 = *Signal of microphone No.1*

2 = *Signal of microphone No.2*

$\overline{\blacksquare}$ = *Rotational tonal component*

$\tilde{\blacksquare}$ = *Non-rotational tonal component*

$\blacksquare'$ = *Broadband component*

$\hat{\blacksquare}$ = *Beamforming operations*

II. Introduction

Due to their advantageous propulsive efficiency properties, Counter-Rotating Open Rotor (CROR) airplane and urban air mobility vehicle engines have been investigated as potential alternatives to some of the current technology used in the aircraft industry [1-4]. Unfortunately, these CROR have some disadvantageous acoustic features which need to be investigated in order to better understand and hence mitigate or even remove the noise sources prior to their widespread application [1-5]. Using single microphone measurements, it has been possible to investigate the noise emission of various setups of a CROR, such as varying blade numbers or rotor locations [6-10]. Using a movable microphone or a linear array of microphones, determining the radiation directivity of the emitted noise for the various configurations has also been possible [6-13]. Furthermore, using a microphone array combined with beamforming technology, the locations of the dominant noise sources can also be investigated and the noise generation mechanisms can be determined [14-20]. Microphone arrays are used to simultaneously record emitted noise with multiple microphones. The microphone signals can be characterized as having given phase and amplitude differences as a result of the microphone locations. The beamforming process corrects for these differences between the signals of the microphones in order to determine the locations of the dominant noise sources [21]. Using the resulting beamforming maps, the locations of the dominant noise sources can be investigated and the noise generation mechanisms can be determined.

The noise of a CROR consists of tonal as well as broadband noise components. The tonal components are present across narrow frequency ranges and usually have large amplitudes. They are generated by the rotation of the blade sets and appear at specific frequencies, which can be calculated from the blade passing frequencies of the rotors. In Ref. [15], the typical tonal noise sources of a CROR have been defined and the investigated frequency bins have been sorted into groups according to their dominant noise generation mechanisms. In Fig. 1, the results of the sorting method can be seen, where the dominant noise sources of each investigated frequency bin have been sorted into given groups of CROR noise sources. The main groups defined in Ref. [15] are rotating coherent noise sources (interaction tones and blade passing frequency tones), shaft order noise sources, and broadband noise sources. Some of the tonal noise sources can be easily identified, due to their special locations on beamforming maps. As an example, interaction tones are in many cases localized to their Mach radii [15-17]. Therefore, they can often be identified and sorted into the correct CROR noise source groups when investigated from the sideline. Unfortunately, this sorting process is very subjective and cannot always accurately identify the mechanism behind the dominant noise source of every

investigated frequency bin. Broadband noise sources are present across a wide frequency range, typically having smaller amplitudes as compared to the tonal noise sources. Therefore, in many cases they are hard to localize as they are below the dynamic range that can be investigated using most beamforming methods. They appear at the real positions of the noise sources, and if the broadband noise source is localized to the same location as a tonal noise source, then it is hard to separate them apart. This causes the subjectivity of the sorting method. In this article a novel beamforming method is presented for isolating the broadband noise generation mechanisms from the tonal ones, making the investigation of these noise sources easier and less subjective.
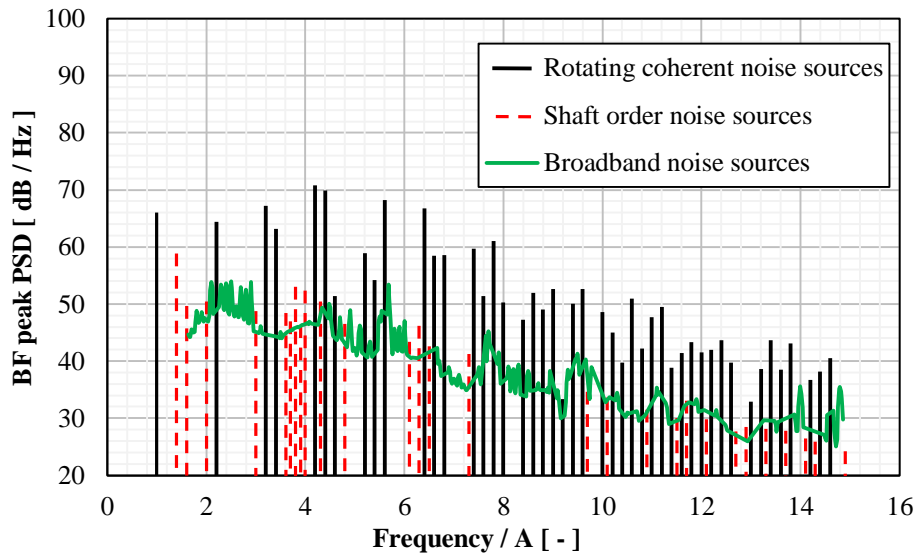

Fig. 1 The result of the sorting method [15]

The broadband noise generation of counter-rotating turbomachinery is similar to the noise generation of airfoils and single stage turbomachinery [19,20,22]. The typical broadband noise sources of CROR are leading edge noise sources, trailing edge noise sources, and blade tip noise sources [3,4,12,17,23-26]. The leading edge noise sources are associated with upstream turbulent flow interacting with the blades. Their frequency range depends on the frequency of the turbulence of the upstream air. For the forward rotor, the amplitude of the turbulence of the upstream flow can be large in the case of approach and takeoff flight conditions (not necessarily the case in a wind tunnel). For the aft rotor, leading edge broadband noise sources can be quite significant due to the effect of the forward rotor on the airflow [12,17,23,26]. The trailing edge noise source is caused by fluctuating blade loading, due to the developed turbulent boundary layer flow passing over the trailing edge [4,12,17,23,24,26]. Trailing edge noise sources are a potentially significant noise source of both the forward and aft rotors. Blade tip noise sources occur when the blade

tip vortices interact with the trailing edges [12,24-26]. According to earlier studies of the investigated geometry and test conditions [17], this type of noise source is not a significant one, as compared to the other broadband noise sources. In Fig. 2 and Fig. 3, the typical locations of the broadband noise sources can be seen for low and high frequencies [17].
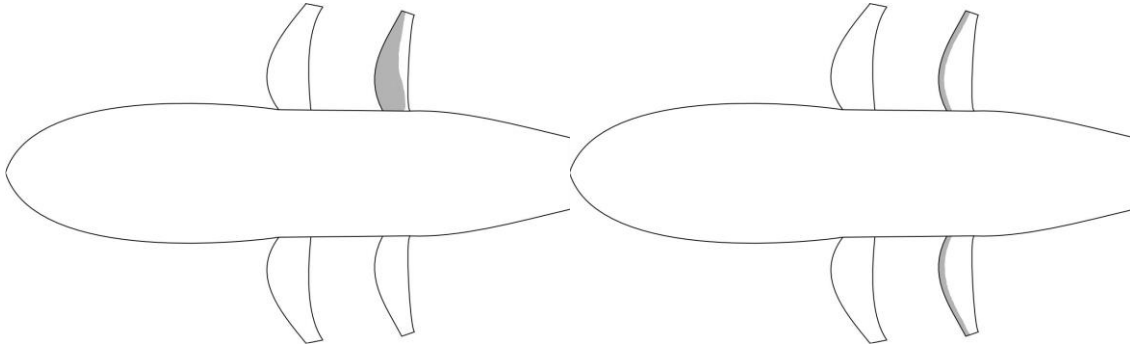

Fig. 2 The typical locations of leading edge broadband noise sources for low (left) and high (right) frequencies
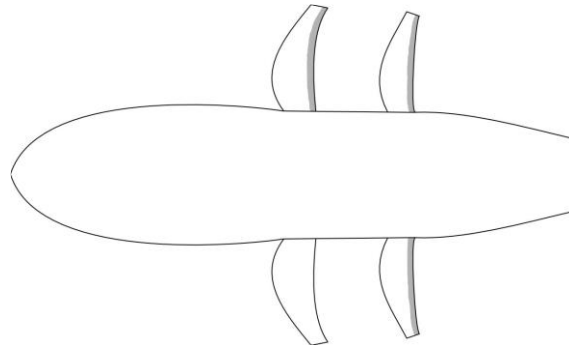
[17]

Fig. 3 The typical locations of trailing edge broadband noise sources [17]

The broadband noise sources described above are hard to investigate due to the presence of tonal noise sources which have larger amplitudes that dominate over the broadband in many frequency bins. In the literature, Sree and Stephens [27,28] have provided a pre-processing method for investigating the broadband spectra of CROR. The method removes the tonal components which are related to the rotational speed from the recorded signal of a microphone. In this study, this pre-processing method is extended in order to account for other tonal noise components and further developed into a beamforming method. As a result, it is now possible to investigate the broadband noise sources for the entire frequency range with beamforming technology.

III. Measurement Setup

In order to investigate the noise of CROR, measurements have been carried out in the NASA Glenn Research Center 9×15 ft Low-Speed Wind Tunnel (LSWT), mounting the investigated rotors on the Open Rotor Propulsion Rig (ORPR) [16, 17]. This can be seen in Fig. 4. Data from the phased array microphone measurements of the test campaign have been processed and presented in this article. The blades under investigation are those of the F31/A31 historical baseline blade set [29]. The forward blade row of the design consists of 12 blades with a diameter of 0.652 m, while the aft rotor has 10 blades with a diameter of 0.630 m.
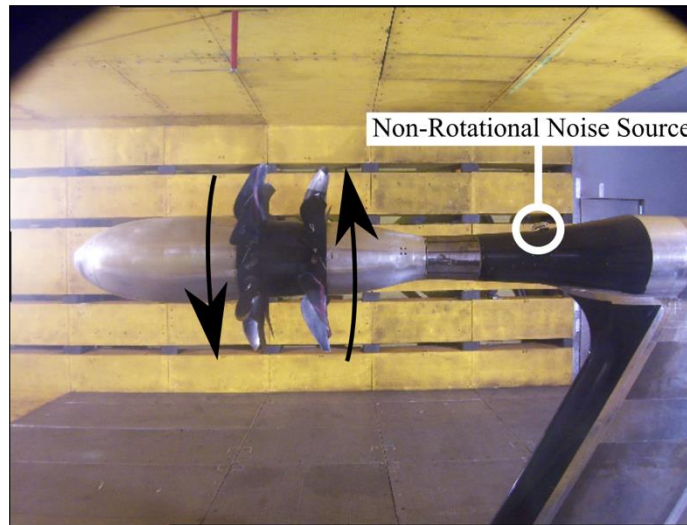

Fig. 4 The view of the camera of the microphone array

The configuration investigated here is the uninstalled design approach condition, with a blade angle of 33.5° on the forward rotor, and a blade angle of 35.7° on the aft rotor. The Mach number of the flow is $M_x = 0.2$, while the angle-of-attack of the flow with regard to the test rig is 0°. The rotational speeds of both rotors have been set equal when corrected for standard day operating conditions, having a value of 5598 rpm. As seen from the upstream direction, the forward rotor rotates in the clockwise direction, and the aft rotor rotates in the counter-clockwise direction (marked in Fig. 4). Further details regarding the test set-up and the test matrix can be found in Ref. [16, 17, 29].

The acoustic measurements have been carried out using the OptiNAV Array48 phased array microphone system [30]. The microphone array has an aperture of 1 m. The signals from the 48 microphones have been simultaneously recorded at a sampling rate of 96 kHz. During the testing, the phased array has been mounted in a cavity along the

southern wall of the wind tunnel facility directly across from the test rig. In order to remove the microphones from the flow, a Kevlar® fabric has been tightly stretched over the opening of the cavity, leaving a gap between the fabric and the phased array. This technique has been developed and tested by others in Ref. [31] and [32], which demonstrated the ability of the technology to improve the signal-to-noise ratio. The signal-to-noise ratio has been further improved by using a long time series (45 s) and removing the diagonal of the cross-spectral matrix during beamforming. During the measurements investigated here, the microphone array has been located at a distance of 1.6 m from the center plane of the test rig, the plane under investigation, which can be considered to be in the acoustic far-field according to simulations carried out by Horváth et al. [16, 17]. An artificial noise source (deer whistle) has been mounted onto the investigated setup in order to verify the beamforming maps, but at the same time it also contaminates the spectral results and beamforming maps. The location of this artificial non-rotational noise source is shown in Fig. 4. In order to remove its effect from the measurement data, the pre-processing method provided in the literature by Sree and Stephens [27, 28] has been extended for noise sources not related to the rotational frequency of the CROR.

IV. Pre-processing of microphone signals

The presence of a large number of tonal components, most of which are associated with the rotational frequencies of the blade sets, makes it difficult to investigate the broadband components. In those frequency bins which are dominated by tonal components, the noise source localizations of the broadband components are in many cases not adequate for carrying out examinations. Therefore, in earlier investigations of the broadband noise of CROR, only those frequency bins have been investigated which are dominated by broadband components. The rotational tonal components appear with large amplitudes at interaction tone frequencies, blade passing frequencies, and shaft order tone frequencies, dominating more than half of the investigated 725 frequency bins of the frequency range from 500 Hz to 15 kHz [15]. Therefore, prior to the investigation of the broadband components, it would be advantageous to remove the tonal components from the recorded signal. In many turbomachinery applications, it is customary to use methods which take a phase average of the data over multiple rotations. This was attempted for CROR data by Sree [27], but it was found that due to jitter, deviations in rotor speed, as well as phase shifts in measured data, the phase averaging methods cannot be used in the case of CROR. Sree and Stephens have developed a signal pre-processing method which can be applied for the emitted noise of CROR [27,28], which removes the tonal components related to

the rotational speed and will be referred to as Rotational Noise Source (RNS) filtering throughout the text. The signal created using this signal pre-processing method will be referred as Single filtered signal throughout the text.

In the case investigated herein, a second tonal component remains in the Single filtered signal, which is not related to the rotational speed of the CROR, but is rather the result of an independent noise generation mechanism, which in this case is a non-rotational noise generation mechanism, a deer whistle. This artificial noise source still contaminates the spectrum of the broadband signal after the RNS filtering, and the broadband component cannot be investigated in those frequency bins, which are dominated by the noise of the deer whistle. In order to generate a signal which only contains information regarding the original broadband component, further signal processing is required. Applying the algorithm of Sree and Stephens [27,28] a second time with appropriate parameters, this second tonal component can also be removed. This second filtering step will be referred to as Non-Rotational Noise Source (NRNS) filtering throughout the text (being that the investigated deer whistle is a non-rotational noise source). The signal which has been pre-processed by the RNS as well as the NRNS filtering method will be referred as the Double filtered signal throughout the text. Figure **5** shows a flow chart of the process of the Double filtering, which is presented in detail in Section IV.A and IV.B. It needs to be stated that though this investigation presents the filtering of the tonal components of the CROR and a deer whistle from the signal, the method is general enough that it can be applied in the removal of other disturbing tonal noise components from the signal.
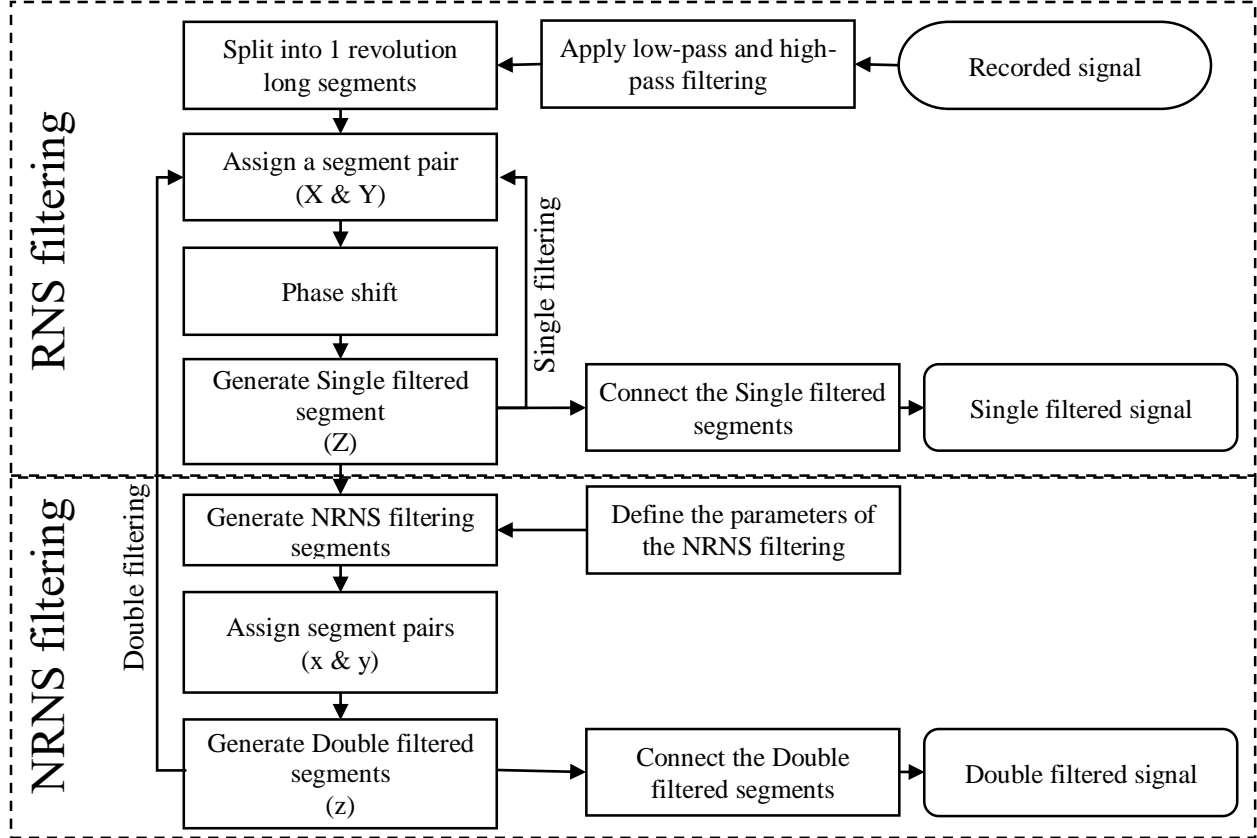
Fig. 5 The process of the Double filtering

A. Removing the tonal noise components that are related to the rotational speed

The method presented herein is based on the subtraction of neighboring segments (X and Y) of the recorded signal of a microphone. According to Ref. [28], the recorded signal must be split into one revolution long segments. One segment consists of tonal components associated with the rotational speed, which will be referred to as RNS components ($\bar{X}$ and $\bar{Y}$), tonal components not associated with the rotational speed, which will be referred to as the NRNS components ($\tilde{X}$ and $\tilde{Y}$) and broadband components (X' and Y'), as seen in Eq. (1) and Eq. (2).

$$X = \bar{X} + \tilde{X} + X' \tag{1}$$

$$Y = \bar{Y} + \tilde{Y} + Y' \tag{2}$$

The RNS component is repeated in every segment of one revolution length of the recorded signal ($\bar{X} = \bar{Y}$). The strength and frequency of NRNS are assumed to be constant throughout the entire signal, but as a result of the splitting

of the signal into one revolution long segments, the phase of this component can differ in equivalent throughout the signal. As a result, this component differs in the neighboring segments ($\tilde{X} \neq \tilde{Y}$). The broadband component is different in the neighboring segments ($X' \neq Y'$). The generated broadband noise is assumed to be statistically constant throughout the recorded signal, which means that its RMS value is constant ($\overline{X'^2} = \overline{Y'^2}$). With the subtraction of two neighboring segments, the RNS component can be removed from the signal, as seen in Eq. (3).

$$X + (-Y) = \bar{X} + \tilde{X} + X' - \bar{Y} - \tilde{Y} - Y' = (\tilde{X} - \tilde{Y}) + (X' - Y') \tag{3}$$

The subtraction of the NRNS component ($\tilde{X} - \tilde{Y}$) behaves like the subtraction of two signals having the same amplitude and frequency, but with different phase, and results in a tonal signal, which has the same frequency as the original NRNS component. The subtraction of the broadband components generates a new broadband signal component ($X' - Y'$). Since the two broadband components are incoherent, the segments should be combined as mean-squared values [28,33]. The RMS value of the generated broadband signal component can therefore be calculated by the Pythagorean relation, as seen in Eq. (4).

$$[RMS(X' - Y')]^2 = [RMS(X')]^2 + [RMS(-Y)']^2 = 2 \cdot [RMS(X')]^2 = 2 \cdot [RMS(Y')]^2 \tag{4}$$

Since the two broadband signal components are expected to have the same RMS amplitudes, the square of the RMS value of the resulting signal is equal to twice the square of the RMS value of the broadband component of the first RNS segment as well as twice the square of the RMS value of the broadband component of the second RNS segment. Therefore, in order for the new broadband component to have the same RMS value as the original broadband component, the resulting signal must be divided by $\sqrt{2}$, as seen in Eq. (5).

$$Z = \frac{X-Y}{\sqrt{2}} = \tilde{Z} + Z' \tag{5}$$

The resulting signal (Z) consists of a NRNS component ($\tilde{Z}$) having the same frequency as the NRNS component of the original signal ($\tilde{X}$ and $\tilde{Y}$), and a broadband component (Z'), which is statistically equivalent to the original broadband component (X' and Y'). Being that the NRNS component will be removed below, steps were not taken in order to correct its amplitude. In Fig. 6. the BeamForm peak (BFpeak) spectrum can be seen as a function of dimensionless frequency, which shows that most of the tonal components have been removed from the signal. The

BFpeak levels are the maximum (peak) beamforming levels calculated by the beamforming method for each frequency bin (each beamforming map). The location of this peak shows the location of the most dominant noise source of the investigated frequency bin. The BFpeak Power Spectral Density (PSD) dB/Hz values are used for presenting the spectral results in this article. The frequency is nondimensionalized by the blade passing frequency of the aft rotor (A). The tonal peaks remaining in the BFpeak spectrum are mostly resulting from noise sources which are not associated with the rotation of the blade sets but rather to other noise sources such as the NRNS located behind the rotors (Fig. 4). Some small tonal peaks of the RNS are still identifiable in the spectrum, but their amplitudes have decreased considerably. The reason behind these remaining peaks will be discussed later on. It will also be seen that the second filtering will almost completely remove these remnants.
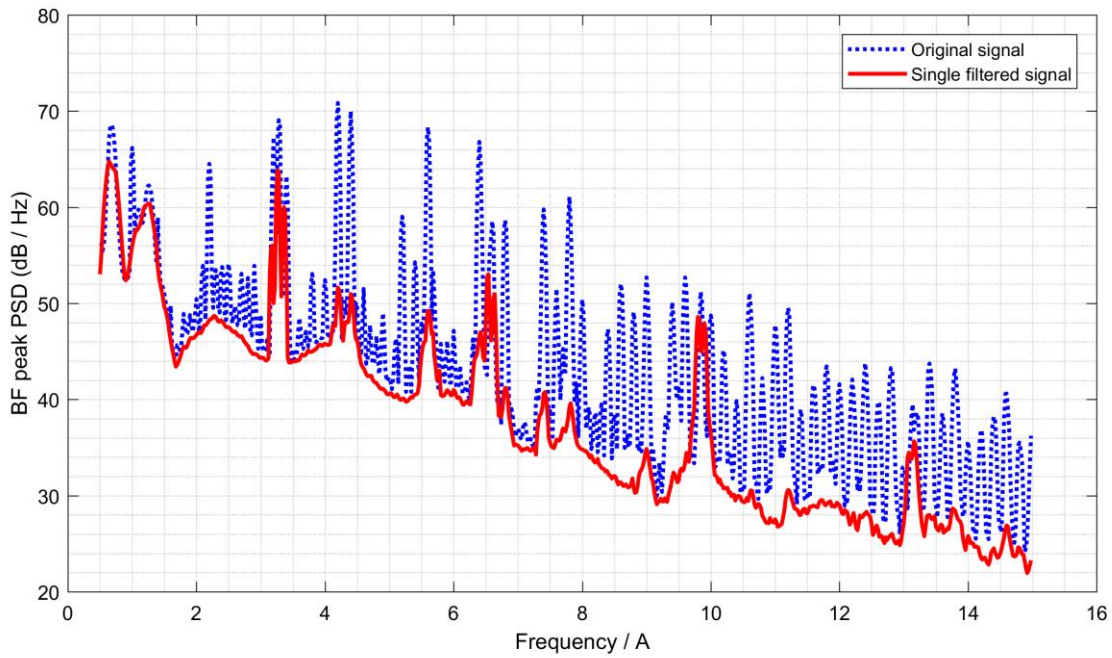

Fig. 6 The BFpeak PSD spectrum of the original signal and the Single filtered signal
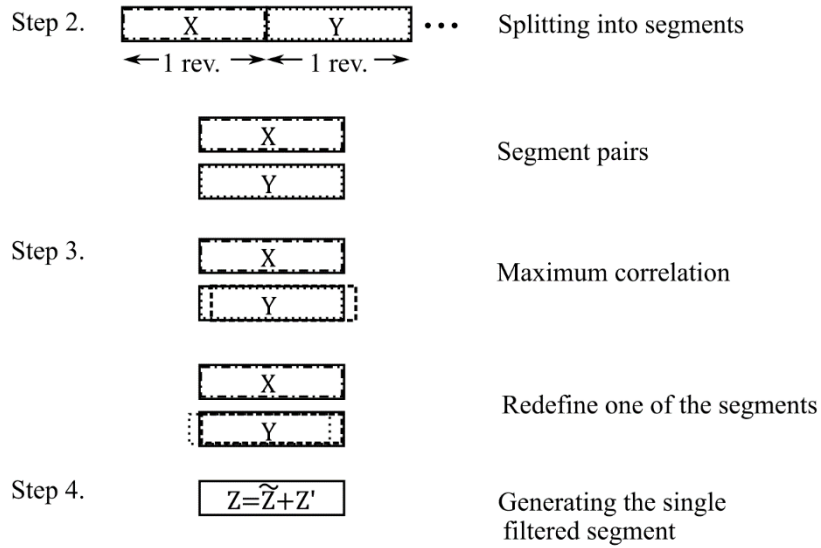
Fig. 7 The process of the RNS filtering

The RNS filtering consists of the following steps: The first step is to filter the recorded signal of a microphone. The interesting part of the signal of the examined CROR appears above 500 Hz, since the blade passing frequencies are around 1 kHz, moreover, below 500 Hz the dominant component of the noise is generated by the wind tunnel [15], which is not investigated in this study. Above 20 kHz the dominant noise sources are not associated with the investigated test rig or rotors and therefore the signal has been filtered below the frequency of 500 Hz and above the frequency of 20 kHz. The second step is to split the recorded signal into one revolution long segments (Fig. 7). The third step is to redefine one of the neighboring segments so that the two segments are in phase. This step corrects for the effect of slight variations of the rotational frequencies of the rotors in time, and therefore the segment subtraction will be performed with maximum correlation. During the phase shift, the method borrows samples from the neighboring segments (Fig. 7). As a result, the measurement data are not corrupted and the tonal components are in the same phase. Step four is performing the subtraction of the segments. According to Eq. (5), a new segment (Z) is generated, which does not contain the RNS component. Step five is to repeat steps 3 and 4 for all of the segment pairs of the original signal. Step six is to apply a Hanning window on the segments in order to guarantee a continuous signal and connect the segments in order to create the Single filtered signal. During the process, one segment is used only once, and therefore, only one new segment (Z) can be generated from two neighboring segments of the original signal (X and Y). The length of the new signal is therefore only half that of the original signal.

B. Removing the non-rotational tonal component

Taking advantage of the properties of the pre-processing method described above, a second, NRNS filtering can be carried out. Considering the remaining tonal component as periodic, appropriate segments can be defined for the filtering of the NRNS component. These new segments will be utilized in removing the undesired non-rotational tonal component from the time signal.

The new segment lengths can be defined based on the frequency of the NRNS ($f = 3129\ Hz$). In defining the segment lengths, one oscillation of the noise source can be considered as one segment. Being that the frequency is relatively high, short segment lengths result in large information loss, and longer segment lengths need to be used. Therefore, in order to apply NRNS filtering, the segment length has to be taken as a multiple of the period of the generating mechanism, which in this case is the period of the noise of the deer whistle. As a result, a longer segment length can be chosen, and the NRNS filtering can be performed. The NRNS component is in the same phase only within one resulting segment of the RNS filtering, and therefore the subtraction of the NRNS filtering can only be performed within one RNS segment. The calculation of the number of samples in a segment (S) can be seen in Eq. (6), where the number of periods, is shown by n, and f_s is the sampling frequency.

$$S = \frac{n}{f} \cdot f_s \tag{6}$$

The maximum number of periods in a NRNS filtering segment (n_{max}) can be determined based on the RNS filtering segment length and the length of a period. The number of periods in a RNS filtering segment (D) can be calculated by Eq. (7), where the period of the revolution (RNS segment length) is divided by the period of the NRNS.

$$D = \frac{1/F}{1/f} \tag{7}$$

The NRNS filtering process requires at least two segments in a RNS filtering segment in order to perform the subtraction, and therefore the maximum number of the periods in a NRNS filtering segment can be calculated using Eq. (8).

$$n_{max} = \frac{D}{2} \tag{8}$$

The NRNS filtering has to be performed after the first four steps of the RNS filtering, after Z has been created. This signal segment contains the broadband component and the NRNS component. The remaining tonal component is in a different phase as compared to the original X and Y segments, but it is constant in the Z segment. Therefore, if the segments (x and y) of the NRNS filtering method are generated from the same Z segment, then the NRNS component can be removed from the signal.
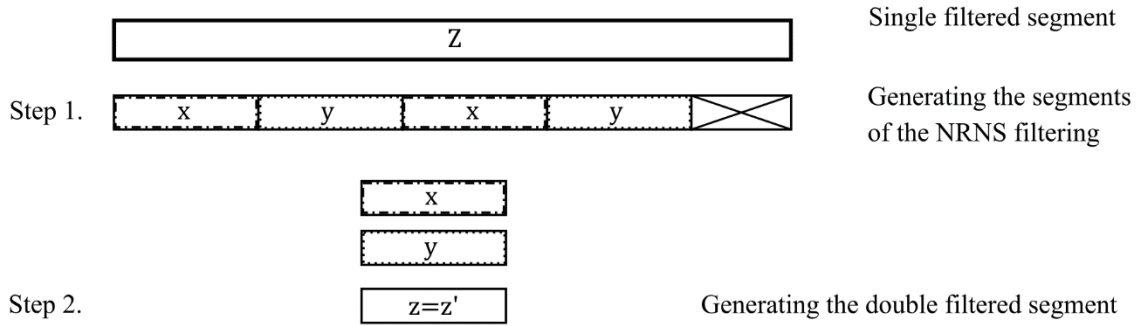
Fig. 8 Steps of the NRNS filtering

Fig. **8** shows the process of the NRNS filtering, which consists of the following steps. The first step is to generate the segments of the NRNS filtering (x and y) from a Single filtered Z segment, which has been generated by the fourth step of the RNS filtering process. The lengths of these segments are n multiples of the period of the non-rotational noise source. These segments contain NRNS components, which are equal in two neighboring segments ($\tilde{x} = \tilde{y}$), since the segment length is equal to a multiple of the period of the generation mechanism, and the statistically equivalent broadband components ($RMS(x') = \mathrm{RMS}(y')$). The NRNS tonal component can be removed by the subtraction of the neighboring segments, as seen in Eq. (9).

$$x + (-y) = \tilde{x} + x' - \tilde{y} - y' = x' - y' \tag{9}$$

The second step is to perform the subtraction of the segments and divide by $\sqrt{2}$ in accordance with Eq. (10), ensuring the statistical equivalence of the new broadband component with the original broadband component.

$$z = \frac{x-y}{\sqrt{2}} = z' \tag{10}$$

The newly generated signal segment (z) only contains information regarding the broadband component of the noise of the investigated CROR. The third step is to repeat steps 3 and 4 of the RNS filtering and the steps of the NRNS filtering for every segment pair of the signal. In step four, a Hanning window having a length equal to that of z' is used in order to guarantee a continuous signal and to connect the segments in generating the resulting broadband signal, which contains information regarding the original broadband component. In Fig. **5**, a flow chart can be seen, which summarizes the entire process of the Double filtering method.

In defining the appropriate segment length for carrying out the NRNS filtering, two separate factors need to be taken into consideration. Examining the spectral results of the cases having various segment lengths for a NRNS frequency of 3129 Hz, the first thing that can be observed is that a shorter segment length results in a more effective filtering. This effect is most likely the result of small changes in the NRNS component. For a longer segment, the change can be more significant between two neighboring segments, and therefore the filtering process is less effective, while for a shorter segment the change can be neglected and a better filtering can be performed. The second factor which influences the effectiveness of the filtering, comes from the fact that we are working with discrete data points. The segment length of the NRNS filtering process is calculated from the period of the NRNS, but the resulting number of data points is rounded to the closest whole number. Therefore, the last period of the tonal component will end with a small phase shift, as seen in Fig. 9, which decreases the effectiveness of the filtering process. This effect can be observed for the higher harmonics, whose period is shorter and the rounding results in a larger phase shift. While in the case of the NRNS, the 96 kHz sampling frequency divided by the frequency of the NRNS results in 31 samples, and a shift of one data point results in an approximately 3 % phase shift for the examined component, the period of the first and second harmonics are 15 and 10 data points, respectively, which results in an approximately 6 % and 10 % phase shift for the examined components. Therefore, the effect of the segment length is examined on the second harmonic at 9387 Hz (9.8 dimensionless frequency) in Fig. 10 a). In Table 1 the segment lengths for various numbers of periods can be seen for the frequency of 3129 Hz, prior to rounding. The examination of the spectral results shows that the magnitude of the rounding error influences the effectiveness of the filtering. On Fig. 10 a), the harmful effects of the rounding error can be observed. While in the case of 7 periods in a NRNS filtering segment, the filtering is successful as a result of the small rounding error, in the case of 8 and 11 periods the tonal peak is not filtered out from the signal, due to the large value of the rounding. This tendency is true in the case of other numbers of periods which are associated with a large rounding error as well. On Figure 10 b), the spectra of the various cases having small

15

rounding errors are shown. Here the tonal peak is successfully filtered from the signal, but the harmful effect of having a long NRNS filtering segment can still be observed. Decreasing the length of the segment results in a better filtering, as can also be concluded from the results in Fig. 10 b).
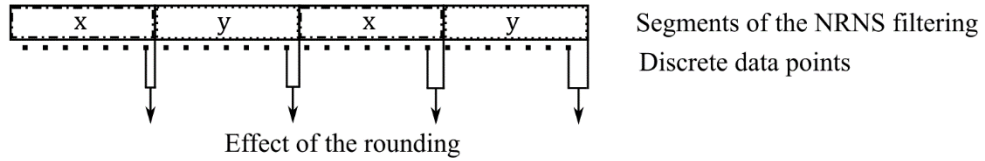

Segments of the NRNS filtering
Discrete data points

Effect of the rounding

Fig. 9 The effect of having discrete data points on the phase of the NRNS component in the NRNS filtering process

Table 1 The segment lengths in the case of various numbers of periods

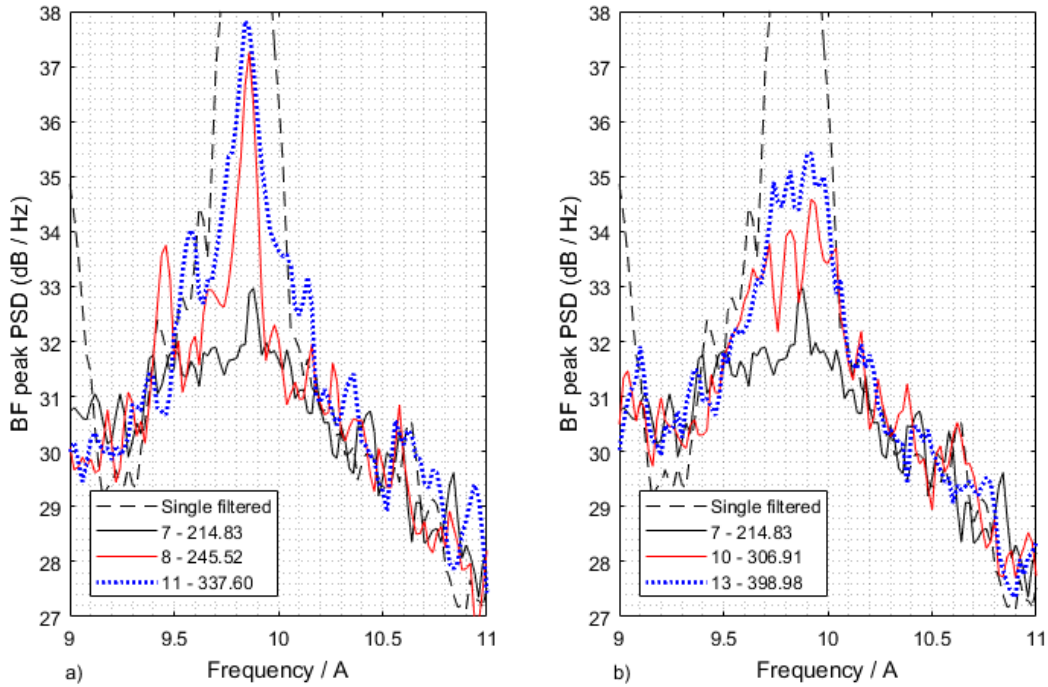| Number of periods	Segment length	Number of periods	Segment length
4	122.76	11	337.60
5	153.45	12	368.29
6	184.14	13	398.98
7	214.83	14	429.67
8	245.52	15	460.36
9	276.21	16	491.05
10	306.91		

Fig. 10 The effect of a) discrete data points and b) the number of periods on the NRNS filtering process

Taking these guidelines into consideration, the favorable number of periods for this test case was determined to be 7. The parameters of the RNS and the NRNS filtering process are summarized in Table **2**, and the spectra of the original, the Single filtered, and Double filtered signal are given in Fig. 11. It can be seen, that the tonal components remaining in the Single filtered signal (both the remaining RNS and the NRNS components) are removed by the NRNS filtering, which results in a signal which contains only the broadband component.

Table 2 The parameters of the filtering processes

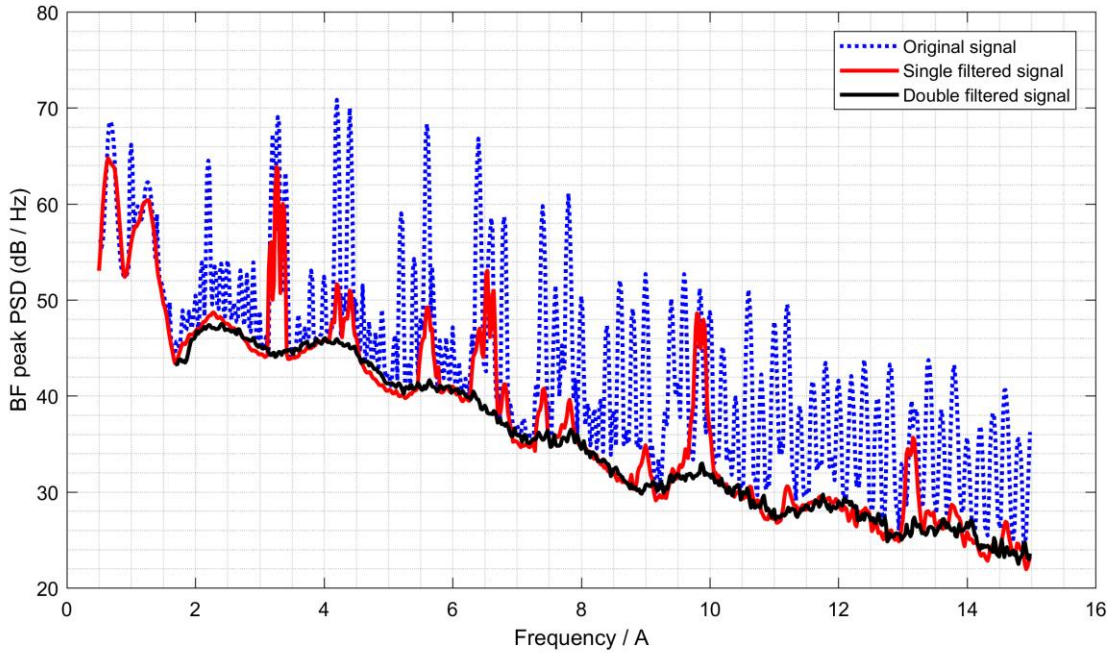|	RNS filtering	NRNS filtering
Generating mechanism of the filterable noise	Rotational	Non-rotational (deer whistle)
Frequency of the generating mechanism (Hz)	95.26	3129
Period of the generating mechanism (s)	0.01049	0.00032
Chosen segment length (s)	0.01049	$7 \cdot 0.00032 = 0.00224$
Number of data points in one segment	1008	215

Fig. 11 The result of the RNS and NRNS filtering

C. Advantages of the pre-processing method

In earlier studies [15,17], our research has shown that there are frequency bins which are dominated by the broadband noise according to the beamforming maps of the original signal. In these frequency bins there are no tonal

components or they are weaker than the broadband components. Figure 12 shows the BFpeak spectrum of the broadband signal of the CROR, plotting those frequency bins which are dominated by the broadband noise and leaving out those bins which are dominated by tonal components [15]. Without the Double filtering, only the broadband noise sources and generation mechanisms of these frequency bins can be investigated. In Fig. 12, the spectrum of the Double filtered signal is also shown. It can be seen that this pre-processed signal has a smoother spectrum with less peaks in it. This is due to the fact that the sorting method is a very subjective method, since distinguishing between tonal and broadband noise sources is not entirely trivial. The Double filtered spectrum does not contain any tonal peaks which are resulting from rotational or non-rotational noise sources, and the filtering process is objective and not influenced by the researchers' decisions. The Double filtered spectrum has a PSD value for every frequency bin of the investigated frequency range, whereas the spectrum of the sorting method consists of only the broadband dominated bins, which is approximately half of the total number of frequency bins.
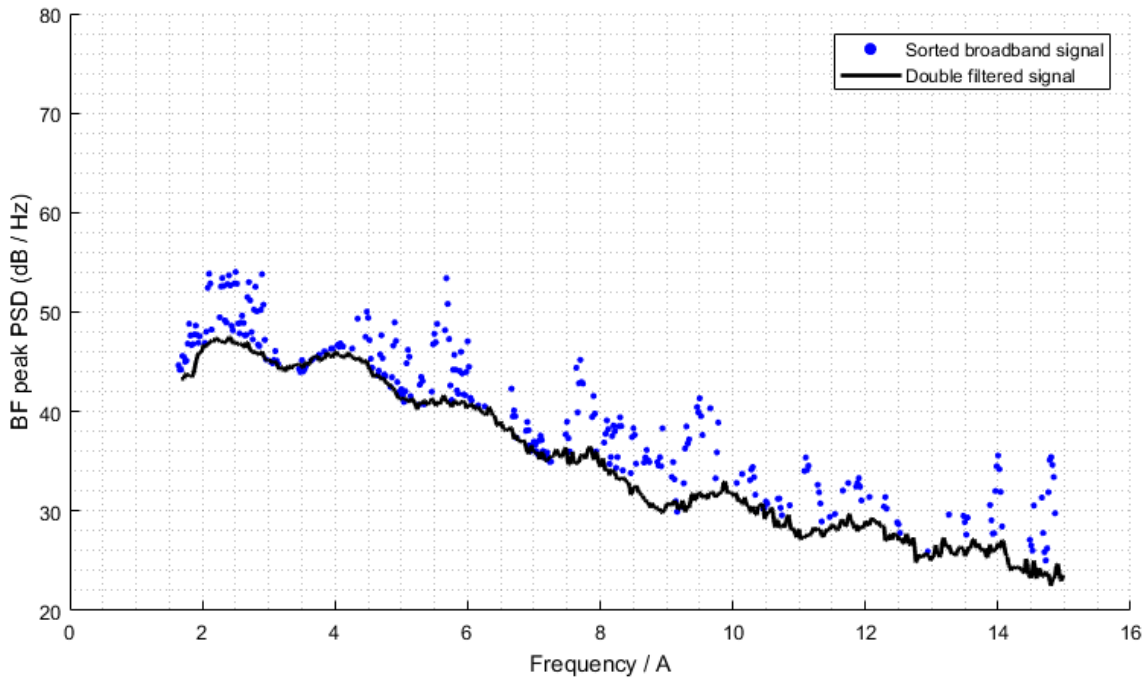

Fig. 12 The broadband spectrum according to the sorting method and the Double filtering pre-processing method

V. Beamforming

Other than the spectral results, the locations of the noise sources also have to be investigated in order to determine the noise generation mechanisms. Beamforming combined with microphone array measurement techniques provides a possible means for investigating the magnitudes and the locations of the noise sources for given frequency bins. In this investigation delay-and-sum beamforming in the frequency domain [21] is applied. This beamforming method has been chosen for this investigation over advanced beamforming methods [35-39], as the experience of the research group has shown that the results provide a set of beamforming maps which can easily be investigated for all categories of CROR noise sources looked at here, as no important information is removed from the beamforming maps while providing an appropriate signal-to-noise ratio. This could not be said for any of the advanced beamforming methods tested during preliminary investigations. In short, the Delay-and-sum processing method works by taking advantage of the phase differences experienced between the signals of various microphones in order to check for possible noise sources in the investigation zone. If a noise source does exist in the investigated point, then the delayed and summed signals result in a large beamforming value on the beamforming maps, while investigated points which do not have any noise sources, have small values on the beamforming maps [21]. The cross-spectral matrices used during the processing of the data are made using a Fast Fourier Transformation (FFT), having a transform length of 4096 with 50% overlap, and 6 dB being subtracted from the results in order to account for the pressure doubling on the surface of the array. The signal-to-noise ratio is further improved by using a long time series (45 s) and removing the diagonal of the cross-spectral matrix during beamforming. The investigation plane is parallel to the plane of the array of the 48 microphones [30] and passes through the axis of the CROR, which is at a distance of 1.6 m. The noise sources were considered as monopoles during the beamforming process.

A. Beamforming of the Double filtered signal

Using the pre-processing method described in Section IV, a broadband signal is generated from the recorded signal of a microphone. The application of the method to the recorded signals of all the microphones of the microphone array results in the broadband signal of every microphone. As a result of the pre-processing, these broadband signals do not contain any tonal components. The generated Double filtered signal is statistically equivalent to the original broadband component, but it is not equal to it [28,34]. Applying beamforming to the Double filtered signal, it is possible to define

the locations of the broadband noise sources. Since the Double filtered signal is only statistically equivalent to the original signal, the validity of these beamforming maps had to be confirmed [34].

For a microphone array consisting of two microphones, X_1 is the first one revolution long segment of the recorded signal of microphone No. 1, and X_2 is that of the recorded signal of microphone No. 2. The second segments of the recorded signals are signed by the letter Y, therefore Y_1 is the second one revolution long segment of the recorded signal of microphone No. 1, and Y_2 is that of the recorded signal of microphone No. 2. These two signal segment pairs, $(X_1; Y_1)$ and $(X_2; Y_2)$, originate from the same noise generation mechanism, but they have different phase and amplitude due to the different locations of the microphones. As described above, this difference is taken advantage of by the beamforming process in localizing the noise sources. The beamforming process performs amplitude corrections in order to decrease the effect of the various losses originating from the various locations of the microphones. The delay-and-sum beamforming method delays the signals, shifting them according to the relative distances between the noise sources and the microphones. As a result, if a true noise source location is investigated, the recorded signals of the microphones of the array will have the best correlation. In this case, $\widehat{X_2}$ is the delayed version of the first segment, and $\widehat{Y_2}$ is the delayed version of the second segment of the recorded signal of microphone No. 2. In this way $(X_1; Y_1)$ and $(\widehat{X_2}; \widehat{Y_2})$ consist of the signals of the same noise generation mechanisms, having the highest correlation. This theory is true for the broadband component of the original signal as well. X_1' and Y_1' are the broadband components of the recorded signals of microphone No. 1, and $\widehat{X'_2}$ and $\widehat{Y'_2}$ are the delayed broadband components of the recorded signal of microphone No. 2, since the broadband components are a part of the original signal. In order to confirm the validity of the beamforming of the Double filtered signal (broadband component), the tonal components are neglected, since the Double filtering process removes the tonal components of the signal (see Eqs. (3) and (9)).

$$Z_1 = Z_1' = \frac{X\prime_1 - Y\prime_1}{\sqrt{2}} = \frac{\widehat{X\prime_2} - \widehat{Y\prime_2}}{\sqrt{2}} = \frac{\widehat{X\prime_2 - Y\prime_2}}{\sqrt{2}} = \widehat{Z'}_2 = \widehat{Z_2} \tag{11}$$

The validity of the RNS filtering is shown in Eq. (11). If the tonal components are neglected ($\overline{X} = \overline{Y} = 0$, $\tilde{X} = 0$ and $\tilde{Y} = 0$), then the result of the RNS filtering (Z) is equal to only its broadband component (Z') and it can be expressed by the broadband components of the original signal (X' and Y'). The broadband component of the recorded signal of microphone No. 1 is equal to the broadband component of the delayed signal of microphone No. 2 ($X_1 = \widehat{X_2}$ and $Y_1 = \widehat{Y_2}$). Therefore, Z_1' can be expressed using $\widehat{X'}_2$ and $\widehat{Y'}_2$, as seen in Eq. (11). The beamforming method

performs the same operations for the entire signal of a microphone, and therefore for each segment of the recorded signal. After rearranging the beamforming operations, it can be seen that the result is equal to the broadband signal of microphone No. 2 ($\widehat{Z'}_2$), and since the tonal components are neglected, it is equal with the segment of the Single filtered signal ($\widehat{Z_2}$), as seen in Eq. (11). This verifies that if there is a noise source localization in the case of the original broadband component, then there will be noise source localization in the case of the Single filtered signal, see Eq. (11).

The validation of the NRNS filtering is similar. If Eq. (11) is true, then there is noise source localization according to the Single filtered signal and there will be noise source localization according to the segments of the NRNS filtering (x and y). The tonal components are still neglected ($\tilde{x} = \tilde{y} = 0$), and therefore the noise source localization can be expressed by the broadband components of the signals (($x'_1; y'_1$) and ($\widehat{x'}_2; \widehat{y'}_2$)). If the tonal components are neglected, then the result of the NRNS filtering (z) is equal to its broadband component (z') and the filtering operation can be expressed by the broadband components of the segments (x' and y'). The broadband component of the Single filtered signal of microphone No. 1 is equal to the broadband component of the delayed signal of microphone No. 2 ($x'_1 = \widehat{x'}_2$ and $y'_1 = \widehat{y'}_2$), and therefore z'_1 can be expressed by $\widehat{x'}_2$ and $\widehat{y'}_2$, as seen in Eq. (12).

$$z_1 = z'_1 = \frac{x'_1 - y'_1}{\sqrt{2}} = \frac{\widehat{x'}_2 - \widehat{y'}_2}{\sqrt{2}} = \frac{\widehat{x'_2 - y'_2}}{\sqrt{2}} = \widehat{z'}_2 = \widehat{z}_2 \qquad (12)$$

The beamforming process performs the same operations on each segment of the recorded signal of a microphone. After rearranging the beamforming operations, it can be seen that the result is equal with the broadband component of the Double filtered signal of microphone No. 2 ($\widehat{z'}_2$), and since the tonal components are neglected, it is equal with the segment of the Double filtered signal (z), as seen in Eq. (12). This verifies the validity of the NRNS filtering method. If there is a noise source localization in the case of the broadband component of the Single filtered signal, then there will be a noise source localization in the case of the Double filtered signal. Thus, if there is a noise source localization according to the broadband component of the original signal, then there will be a noise source localization in the case of the Double filtered signal. This theory can be extended to every microphone of the microphone array. As a result, it is possible to use the newly generated broadband signals for beamforming and investigating the broadband noise sources on beamforming maps.

22

B. Beamforming maps

The beamforming maps show the locations of the most dominant noise sources, which are generated by the strongest noise generation mechanisms of an investigated frequency bin. The localized noise sources on the beamforming maps depend on the location of the generation mechanism, the directivity of the noise source, and the direct sight of the microphones onto the noise source. The noise sources of the aft rotor appear above the shaft if the most dominant noise generation mechanism is on the suction side of the blades, because the microphones see them directly. They appear below the shaft if the most dominant noise generation mechanism is on the pressure side of the blades, because the microphones see those directly. It is vice versa in the case of the forward rotor. The noise sources appear above the shaft if the most dominant noise generation mechanism is on the pressure side of the blades, because the microphones see them directly, and they appear below the shaft if the most dominant noise generation mechanism is on the suction side of the blades, because the microphones see those directly.

The dominant noise sources of the investigated frequency bins can be examined on the beamforming maps of the original signals. As a result of the Double filtering, it possible to investigate the broadband noise sources on the beamforming maps in greater detail. In Fig. 13, a beamforming map can be seen of a frequency bin which was originally dominated by a tonal interaction tone noise source. The tonal component was filtered by the RNS filtering process, since the dominant noise source was a RNS, and it is now possible to localize the broadband noise sources. The beamforming maps of the Single filtered and the Double filtered signals are almost equal, which means that the second filtering process did not disturb the localization of the broadband noise sources.
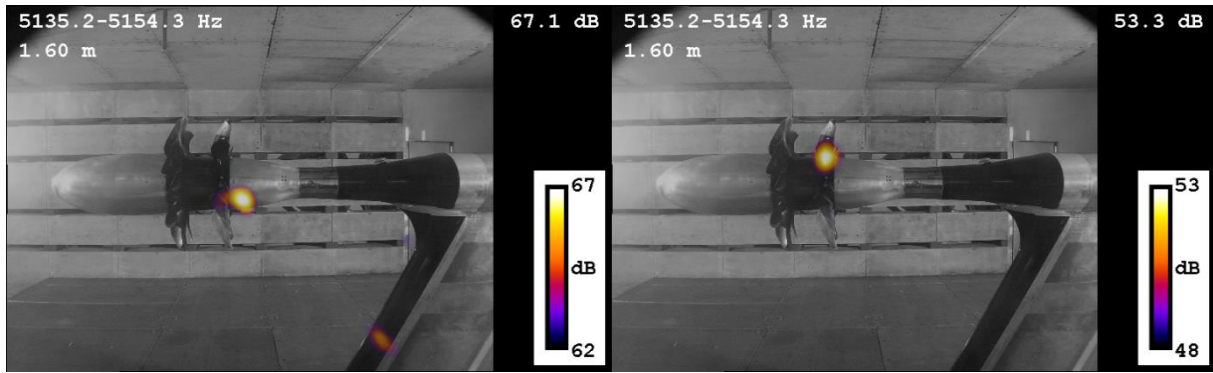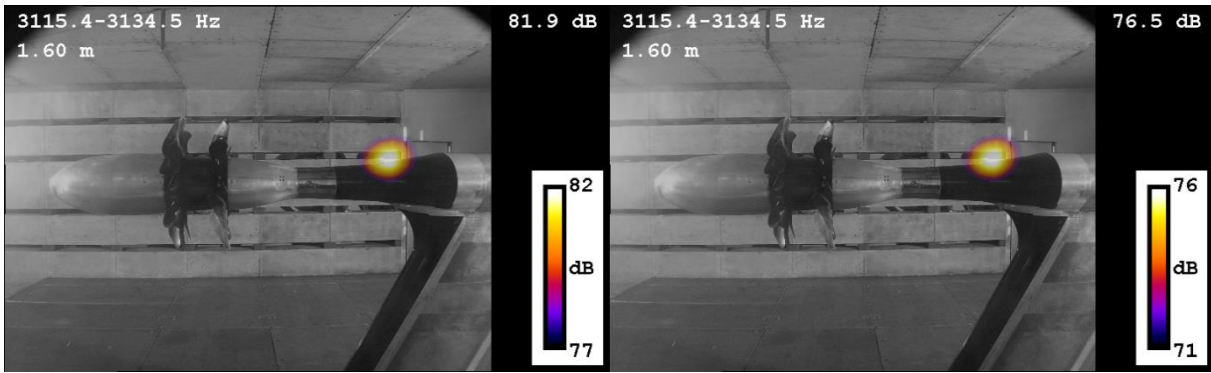
a) Original signal

b) Single filtered signal
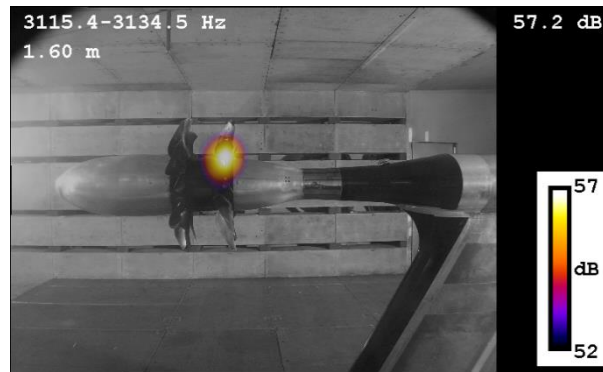

c) Double filtered signal

Fig. 13 The beamforming maps of an interaction tone noise source which is removed by the filtering in the frequency bin 5135.2-5154.3 Hz

In Fig. 14, the beamforming maps of a frequency bin which was originally dominated by the noise of the non-rotational noise source can be seen. The figure shows that the noise source is not localized onto the CROR, but onto the NRNS, which is located behind the rotors, both in the case of the original and Single filtered signal, since the RNS filtering process did not remove the effect of the NRNS. The NRNS filtering was able to remove the effect of the NRNS, and therefore the broadband component of this frequency bin can be investigated.
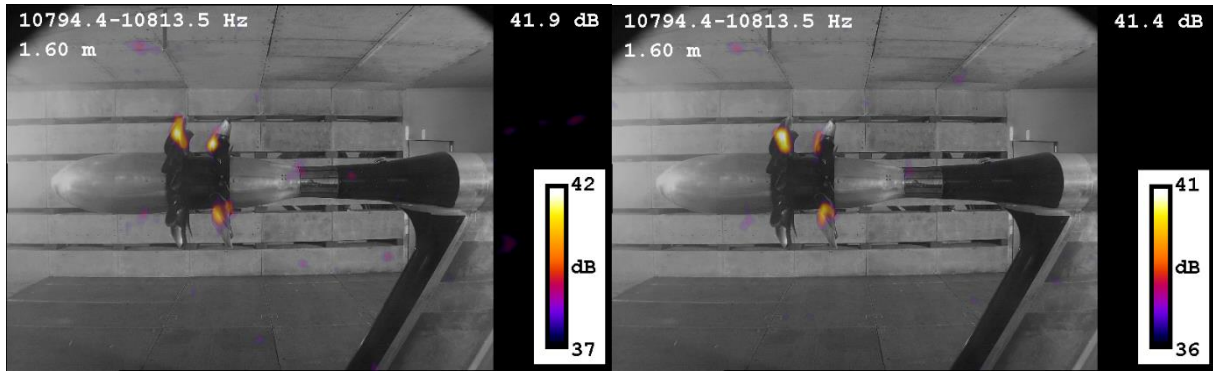
a) Original signal

b) Single filtered signal

c) Double filtered signal

Fig. 14 The beamforming maps of the frequency of the NRNS in the frequency bin 3115.4-3134.5 Hz

In Fig. 15, a beamforming map can be seen of a frequency bin which was originally dominated by a broadband noise source. As can be seen, the maps are almost the same, and the filtering process did not change the localization of the broadband component.

25

a) Original signal

b) Single filtered signal

c) Double filtered signal

Fig. 15 The beamforming maps of a broadband noise source in the frequency bin of 10794.4-10813.5 Hz

In accordance with earlier studies [15,17], which examined only those bins which are dominated by the broadband components of the original signal, the broadband noise sources appear on the trailing edge of the forward rotor and on the leading and trailing edges of the aft rotor. For low frequencies (below 6 kHz), the beamforming maps are quite similar to the beamforming maps of the broadband bins of the original signal. As a result of the Double filtering, the typical broadband noise sources can be investigated in those frequency bins which were originally dominated by a tonal noise source. In this low frequency range, the broadband noise sources are localized to the leading edges of the blades of the aft rotor on the suction side (see Fig. 16). Above 6 kHz, beside the leading edge noise source of the aft rotor, a noise source appears at the root of the suction side of the blades and on the trailing edge of the pressure side of the blades of the forward rotor (see Fig. 17). These noise sources went unnoticed on the beamforming maps of the original signal. At high frequencies (above 10 kHz), the noise sources on the pressure side of the trailing edge of the forward rotor and the leading edges of both the pressure and suction sides of the aft rotor are typical noise sources (see Fig. 18). No dominant noise sources were localized to the suction side of the forward rotor.

Fig. 16 Typical leading edge noise source of the aft rotor at low frequencies in the case of the Double filtered signal

Fig. 17 Typical trailing edge noise source of the forward rotor and leading edge noise source of the aft rotor at mid frequencies in the case of the Double filtered signal
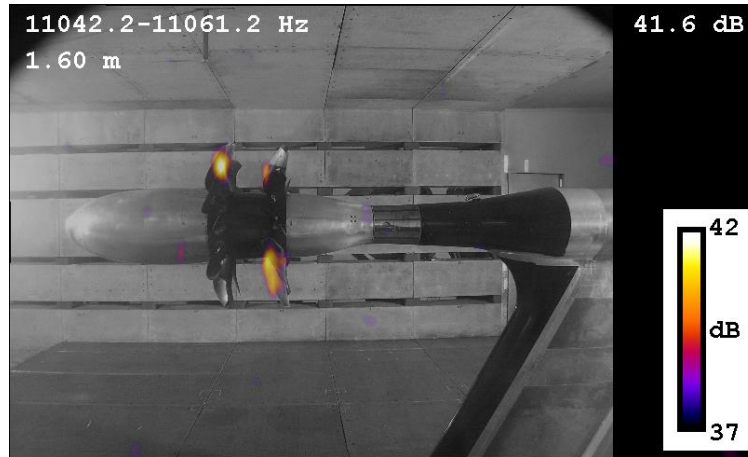
Fig. 18 Typical trailing edge noise source of the forward rotor and the leading edge noise source of the aft rotor at high frequencies in the case of the Double filtered signal

VI. Conclusion

CROR are receiving significant attention due to their exceptional propulsive efficiency properties which come hand in hand with their noise emission issues. While microphone array measurements and beamforming technology have provided a possible means for localizing the dominant noise sources of CROR, the higher levels associated with tonal noise sources have, till now, made it difficult to study the broadband noise sources in greater detail. In this study a pre-processing method for separating apart the broadband noise from the recorded signal has been further developed and combined with beamforming. The locations of the broadband noise sources can now be investigated in every frequency bin across the entire spectrum. The typical broadband noise sources agree with those which were determined during earlier studies, such as the trailing edge noise sources of the forward rotor and the leading and trailing edge noise sources of the aft rotor, but can now be investigated in greater detail, making the evaluation of the results less subjective and hence easier to carry out. After removing the noise sources that are related to the rotational speed, a second tonal component can remain in the new signal. As an example, this paper investigated the noise of a deer whistle mounted in the test section. The effect of this non-rotational noise source has been successfully filtered from the signal using a further development of the filtering method. Using the period of the non-rotational noise source, new parameters can be defined and a filtering can be performed. The Double filtering process can therefore be used to remove these further tonal components from the signal, and the beamforming of the Double filtered signal results in beamforming maps which contain only the broadband noise sources in all the frequency bins which were dominated

by some sort of tonal components in the beamforming maps of the original signal. With the help of Double filtering, greater insight can be reached into the broadband noise generation mechanisms of CROR, which will help reduce their noise emission levels through better designs.

Acknowledgments

References

[1] Bowles, M. D., " "Apollo" of Aeroacoustics: NASA's Aircraft Energy Efficiency Program 1973-1987," NASA Headquarters, Washington, D.C., USA, 2010, 113-140.

[2] Woodward, R. P., "Noise of a Model High Speed Counterrotation Propeller at Simulated Takeoff/Approach Conditions (F7/A7)," NASA TM-100206, 1987, doi: https://doi.org/10.2514/6.1987-2657

[3] Blandeau, V. P., Joseph, P. F., "Broadband Noise Due to Rotor-Wake/Rotor Interaction in Contra-Rotating Open Rotors," AIAA Journal, Vol. 48, No. 11, November 2010, doi: https://doi.org/10.2514/1.J050566

[4] Blandeau, V. P., Joseph, P. F., Kingan, M. J., Parry A. B., "Broadband Noise Predictions from Uninstalled Contra-Rotating Open Rotors," *International Journal of Aeroacoustics*, Vol. 12, No. 3, 2013. Pp. 245-282, doi: https://doi.org/10.1260/1475-472X.12.3.245

[5] Peake, N. and Parry, A. B., "Modern Challenges Facing Turbomachinery Aeroacoustics," *Annual Review of Fluid Mechanics*, Vol. 44(1), pp. 227-248., 2012, doi: https://doi.org/10.1146/annurev-fluid-120710-101231

[6]   Woodward, R. P., "Noise of a Simulated Installed Model Counter-Rotation Propeller at Angle-of-Attack and Takeoff/Approach Conditions," Aerospace Sciences Meeting, Reno, NV, USA, AIAA-90-0283, 1990, doi: https://doi.org/10.2514/6.1990-283

[7]   Woodward, R. P. and Gordon, E. B., "Noise of a Model Counterrotation Propeller with Reduced Aft Rotor Diameter at Simulated Takeoff/Approach Conditions (F7/A3)," *Aerospace Sciences Meeting*, Reno, NV, USA. AIAA-88-0263, 1988, doi: https://doi.org/10.2514/6.1988-263

[8]   Woodward, R. P., Hall, D. G., Podboy, G. G., et al., "Takeoff/Approach Noise of a Model Counterrotation Propeller with a Forward-Swept Upstream Rotor," *Aerospace Science Meeting and Exhibition*, Reno, NV, USA, AIAA-93-0596, 1993, doi: https://doi.org/10.2514/6.1993-596

[9]   Woodward, R. P. and Hughes, C. E., "Noise of a Model Counterrotation Propeller with Simulated Fuselage and Support Pylon at Takeoff/Approach Conditions," *AIAA 12th Aeroacoustics Conference*, San Antonio, TX, USA, AIAA-89-1143, 1989, doi: https://doi.org/10.2514/6.1989-1143

[10]   Parry, A. B. and Crighton, D. G., "Prediction of Counter-Rotation Propeller Noise," *AIAA 12th Aeroacoustics Conference*, San Antonio, TX, USA, AIAA-89-1141, 1989, doi: https://doi.org/10.2514/6.1989-1141

[11]   Elliott, D. M., "Initial Investigation of the Acoustics of a Counter Rotating Open Rotor Model With Historical Baseline Blades in a Low Speed Wind Tunnel," *17th AIAA/CEAS Aeroacoustics Conference*, Portland, OR, USA, AIAA 2011-2766, 2011, doi: https://doi.org/10.2514/6.2011-2760

[12]   Kennedy, J., Eret, P., Bennett, G., Sopranzetti, F., Chiariotti, P., Castellini, P., Finez, A., and Picard, C., "The Application of Advanced Beamforming Techniques for the Noise Characterization of Installed Counter Rotating Open Rotors," *19th AIAA/CEAS Aeroacoustics Conference*, AIAA 2013-2093. May 2013, doi: https://doi.org/10.2514/6.2013-2093

[13]   Fenyvesi, B., Kriegseis, J. and Horváth, Cs., "Application of a Combined Method for the Investigation of Turbomachinery Noise Sources: Beamforming and Proper Orthogonal Decomposition," *25th AIAA/CEAS Aeroacoustics Conference*, AIAA 2019-2637, Delft, The Netherlands, May 2019, doi: 10.2514/6.2019-2637

[14]   Funke, S., Kim, L. and Siller, H. A., "Microphone-Array Measurements of a Model Scale Contra-Rotating Open Rotor in a Reverberant Open Wind-Tunnel," *17th AIAA/CEAS Aeroacoustics Conference*, Portland, OR, USA, AIAA 2011-2766, 2011, doi: https://doi.org/10.2514/6.2011-2766

[15]   Fenyvesi, B., Tokaji, K. and Horváth, Cs., "Investigation of a Pylons Effect on the Character of Counter-Rotating Open Rotor Noise using Beamforming Technology," *Acta Acoustica United with Acoustica*, vol. 105 (1), pp. 56-65, 2019, doi: https://doi.org/10.3813/AAA.919287

[16]   Horváth, Cs., Envia, E. and Podboy G. G., "Limitations of Phased Array Beamforming in Open Rotor Noise Source Imaging," *AIAA Journal*, Vol. 52, No. 8, 2014, pp. 1810-1817, doi: https://doi.org/10.2514/1.J052952

[17]   Horváth, Cs., "Beamforming Investigation of Dominant Counter-Rotating Open Rotor Tonal and Broadband Noise Sources," *AIAA Journal*, Vol. 53, No. 6, 2015, pp. 1602-1611, doi: https://doi.org/10.2514/1.J053465

[18]   Chiariotti, P., Martarelli, M., Tomasini, E. P., et al., "Aeroacoustic Source Localization on Open Rotor Aircraft Model in Wind Tunnel Tests," 43rd International Congress on Noise Control Engineering, Melbourne, Australia, 2014.

[19]   Balla E, Vad J., "Establishment of a Beamforming Dataset on Basic Models of Low-Speed Axial Fan Blade Sections," *Periodica Polytechnica-Mechanical Engineering*, 2017; 61:(2) pp. 122-129, doi: https://doi.org/10.3311/PPme.9548

[20]   Benedek, T., Vad, J., "An Industrial Onsite Methodology for Combined Acoustic-Aerodynamic Diagnostics of Axial Fans, Involving the Phased Array Microphone Technique," *International Journal of Aeroacoustics*, 2016, 15.1-2: 81-102, doi: https://doi.org/10.1177/1475472X16630849

[21]   Mueller, T. J., "Aeroacoustic Measurements," Springer-Verlag, Berlin, Germany, 2002, doi: https://doi.org/10.1115/1.1584413

[22]   Brooks, T. F., Pope, D. S., Marcolini, M. A. "Airfoil self-noise and prediction," NASA Reference Publication NASA-RP-1219. 1989.

[23]   Blandeau, V. P., "Aerodynamic Broadband Noise from Contra-Rotating Open Rotors," PhD Dissertation, University of Southampton, 2011.

[24]   Hubbard, H. H., "Aeroacoustics of Flight Vehicles: Theory and Practice," NASA-RP-1258-VOL-1, 1991.

[25]   Moreau, S., Roger, M., "Advanced Noise Modeling for Future Propulsion Systems," *International Journal of Aeroacoustics*, Vol. 17, No. 6-8, 2018, pp.579-599, doi: https://doi.org/10.1177/1475472X18789005

[26]   Kingan, M. J., "Open Rotor Broadband Interaction Noise," *Journal of Sound and Vibration*, Vol. 332, No. 17, 2013, pp. 3956-3970, doi: https://doi.org/10.1016/j.jsv.2013.03.014

[27]   Sree, D., "A Novel Signal Processing Technique for Separating Tonal and Broadband Noise Components from Counter-Rotating Open-Rotor Acoustic Data," *International Journal of Aeroacoustics*, Vol. 12, No. 1-2, 2013, pp. 169-188, doi: https://doi.org/10.1260/1475-472X.12.1-2.169

[28]   Sree D. and Stephens D. B., "Improved Separation of Tone and Broadband Noise Components from Open Rotor Acoustic Data," *Aerospace*, Vol. 3, No. 3, 2016. doi:10.3390/aerospace3030029

[29]   Van Zante, D. E., Gazzaniga, J. A., Elliott, D. M., et al., "An Open Rotor Test Case: F31/A31 Historical Baseline Blade Set," *20th International Symposium on Airbreathing Engines*, Gothenburg, Sweden, ISABE 2011-1310, 2011.

[30]   Optinav Inc., Array 48, http://www.optinav.info/Array48.pdf, 2017.

[31]   Jaeger, S. M., Horne, W. C., Allen, C. S., "Effect of Surface Treatment on Array Microphone Self-Noise," *6th AIAA/CEAS Aeroacoustics Conference and Exhibit*, Lahaina, Hawaii, USA, AIAA 2000-1937, 2000, doi: https://doi.org/10.2514/6.2000-1937

[32] Fleury, V., Coste, L., Davy, R., "Optimization of Microphone Array Wall Mountings in Closed-Section Wind Tunnels," *AIAA Journal*, Vol. 50, No. 11, 2012, pp. 2325-2335, doi: https://doi.org/10.2514/1.J051336

[33] Puckette, M., "The Theory and Technique of Electronic Music," World Scientific Publishing, May 2007, doi: https://doi.org/10.1142/6277

[34] Tokaji, K. and Horváth, Cs., "Combining Signal Pre-Processing Methods with Beamforming for Broadband Turbomachinery Applications," *Berlin Beamforming Conference*, BeBeC-2018-D28, 2018.

[35] Sijtsma, P., "CLEAN Based on Spatial Source Coherence," *13th AIAA/CEAS aeroacoustics conference*, Rome, Italy, 21–23 May 2007, paper no. AIAA 2007-3634, doi: https://doi.org/10.2514/6.2007-3436

[36] Yardibi, T., Zawodny NS., Bahr C., Liu F., Cattafesta L. N. and Li. J., "Comparison of Microphone Array Processing Techniques for Aeroacoustic Measurements," *International Journal of Aeroacoustics,* 2010, Vol. 9, No. 6, pp. 733–762, doi: https://doi.org/10.1260/1475-472X.9.6.733

[37] Dougherty R. P., "Functional Beamforming," *Berlin Beamforming Conference,* Berlin, Germany, February 2014, BeBeC-2014-01

[38] Brooks, T. F., Humphreys, W. M., "A Deconvolution Approach for the Mapping of Acoustic Sources (DAMAS) Determined from Phased Microphone Arrays," *Journal of Sound and Vibration*, Vol. 294, No. 4–5, July 2006, pp. 856-879., doi:10.1016/j.jsv.2005.12.046

[39] Merino-Martínez, R., Sijtsma, P., Snellen, M. et al., "A review of acoustic imaging methods using phased microphone arrays," *CEAS Aeronautical Journal*, vol. 10, 2019, pp. 197–230, doi: https://doi.org/10.1007/s13272-019-00383-4